

**OPEN ACCESS**

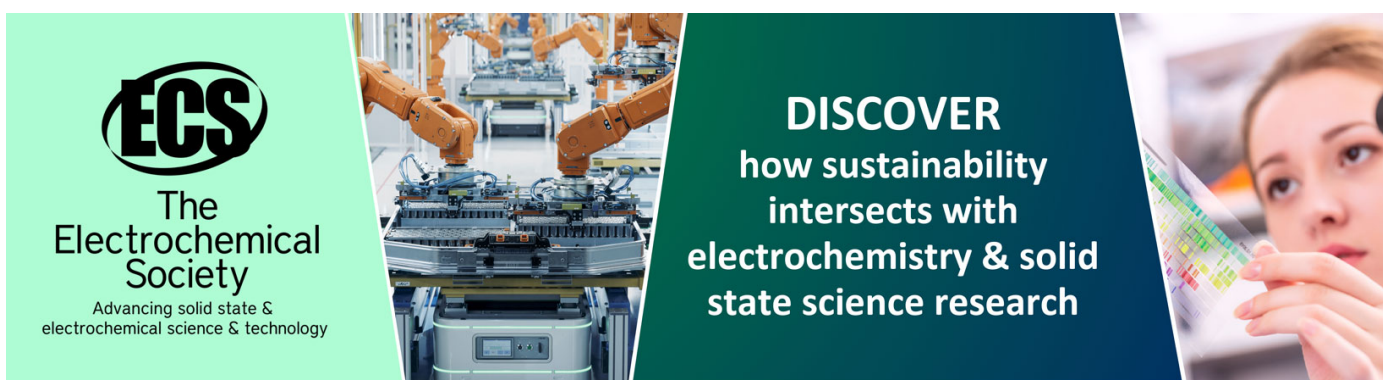
## Some insight into the convergence of the multiple scattering series expansion

To cite this article: Didier Sébilleau and Calogero R Natoli 2009 *J. Phys.: Conf. Ser.* **190** 012002

View the [article online](#) for updates and enhancements.

### You may also like

- [Automated screening of AURKA activity based on a genetically encoded FRET biosensor using fluorescence lifetime imaging microscopy](#)  
Florian Sizaïre, Gilles Le Marchand, Jacques Pécréaux et al.
- [Flexural strength improvement for structural glass: a numerical study](#)  
R Hin, K Cheng, V Han et al.
- [Parallel use of a convolutional neural network and bagged tree ensemble for the classification of Holter ECG](#)  
Filip Plesinger, Petr Nejedly, Ivo Viscor et al.



**ECS**  
The  
Electrochemical  
Society  
Advancing solid state &  
electrochemical science & technology

**DISCOVER**  
how sustainability  
intersects with  
electrochemistry & solid  
state science research

# Some insight into the convergence of the multiple scattering series expansion

Didier Sébilleau<sup>1</sup> and Calogero R. Natoli<sup>2</sup>

<sup>1</sup> Équipe de Physique des Surfaces et des Interfaces,  
Institut de Physique de Rennes, UMR CNRS-UR1 6251,  
Université de Rennes-1, 35042 Rennes-Cedex, France

<sup>2</sup> Laboratori Nazionali di Frascati, INFN,  
via Enrico Fermi 40, I-00044 Frascati, Italy

E-mail: [didier.sebilleau@univ-rennes1.fr](mailto:didier.sebilleau@univ-rennes1.fr)

**Abstract.** We explore the convergence of the multiple scattering series by studying the spectral radius of the corresponding multiple scattering matrix. The energy variations of this spectral radius exhibit strong oscillations. These oscillations are shown to depend strongly on the electronic and crystallographic structure in the low energy regime. As the calculation of the eigenvalues of the multiple scattering matrix is very long, we devise a fast algorithm to approximate this spectral radius.

**PACS numbers :** 02.10.Yn, 61.05.jd

## 1. Introduction

Multiple scattering (MS) theory has a longstanding history in physical and chemical sciences. It is now used to describe both the internal structure and spectroscopic experiments in fields as different as nuclear physics, molecular physics or condensed matter physics and chemistry. It is its unique ability to describe in a rather straightforward and physically transparent way the interaction of a particle of any kind with a surrounding or external medium whose underlying structure can be decomposed into independent potentials that makes it so appealing and powerful for the accurate description of many phenomena.

Although its basics are well understood, the practical implementation of MS theory comes more and more across computational bottlenecks with the ever increasing number of potentials that need to be incorporated into a calculation to satisfactorily describe more and more complex phenomena or materials. In condensed matter physics for instance, the description of nanostructured objects, whose size can be very large compared to interatomic distances, often requires thousands of atoms to reach a proper description. It is then necessary to have a better control on the algorithms used to implement MS so as to avoid the computational bottlenecks we have mentioned above.

There are several formulations of MS theory in the literature, but one we find particularly convenient is that based on the scattering path operator formulation [1, 2], which can be used, in condensed matter theory, both for bandstructure calculations and to model a large range of spectroscopies [3], and especially synchrotron radiation-based experiments. Within this particular approach, the scattering path operator can be viewed as the operator describing all the processes

that a given particle undergoes while going from one atom to another, taking fully into account the whole structure of the material. This operator contains therefore all the information (both structural and electronic/magnetic) in the neighborhood of this particle (close neighborhood or large depending essentially on the kinetic energy of the probe particle).

Technically speaking, if we represent the potential describing the interaction of the probe particle with atom  $i$  as  $V_i$  and the propagator describing the behaviour of this probe within the material under study by  $G$ , we can define the scattering path operator as

$$\bar{\tau}^{ji} = \bar{V}_i \delta_{ji} + \bar{V}_j G \bar{V}_i \quad (1)$$

Here, the overbar is simply a remainder that, because atom  $i$  and atom  $j$  do not necessarily coincide with the arbitrary origin we choose, the corresponding operator contains translation operators referring to this origin.

As illustrated in detail in reference [3], all the spectroscopies using one or several electrons to probe the matter can be described using this scattering path operator. For instance, the cross-section of low-energy electron diffraction (LEED) or valence photoelectron diffraction (valence PED) can be expressed as a function of  $\bar{\tau}^{ji}$  with  $i$  and  $j$  scanning the material while that of core PED is directly related to  $\bar{\tau}^{j0}$  where 0 is the atom where the core excitation takes place. Likewise, X-ray absorption spectroscopy (XAS) depends only on  $\bar{\tau}^{00}$  and the electron energy loss spectroscopy (EELS) cross-section involves three scattering path operators at three different energies (one per electron contributing to the physical process).

Computationally speaking, equation (1) is not convenient and it is normally replaced by the equation of motion satisfied by this scattering path operator

$$\begin{cases} \bar{\tau}^{ji} = \bar{T}_i \delta_{ji} + \sum_{k \neq j} \bar{T}_j G_o \bar{\tau}^{ki} \\ \bar{\tau}^{ji} = \bar{T}_i \delta_{ji} + \sum_{k \neq i} \bar{\tau}^{jk} G_o \bar{T}_i \end{cases} \quad (2)$$

$\bar{T}_i$  is the usual atomic scattering operator associated to potential  $\bar{V}_i$ , and  $G_o$  the free electron propagator.

A formulation such as (2) provides directly two straightforward ways to implement the computation of this scattering path operator. One is to factorize this equation of motion. Using bold characters to represent matrices, this leads to the so-called full MS formulation

$$\boldsymbol{\tau} = (\boldsymbol{T}^{-1} - \boldsymbol{G}_o)^{-1} = \boldsymbol{T}(\boldsymbol{I} - \boldsymbol{G}_o \boldsymbol{T})^{-1} = (\boldsymbol{I} - \boldsymbol{T} \boldsymbol{G}_o)^{-1} \boldsymbol{T} \quad (3)$$

In this case, the core of the algorithm consists in the inversion of the multiple scattering matrix  $(\boldsymbol{T}^{-1} - \boldsymbol{G}_o)^{-1}$ . This matrix will become large very quickly when increasing the energy and the number of atoms involved in the description of the material. Furthermore, it is not sparse, so that the inversion process will scale as  $N^2$  for the memory and  $N^3$  for the CPU time, when  $N$  is the dimension of the matrix. Despite being the best approach from a scattering point of view where it gives an exact result, it is restricted to low energies and relatively small clusters.

An alternative to this algorithm is to iterate the equation of motion. This gives

$$\bar{\tau}^{ji} = \bar{T}_i \delta_{ji} + \bar{T}_j G_o \bar{T}_i + \sum_{k \neq i} \bar{T}_j G_o \bar{T}_k G_o \bar{T}_i + \dots \quad (4)$$

which, when rewritten into matrix form is formally equivalent to the Taylor expansion of equation (3). We know that such an expansion is only valid if it converges, in which case its limit is indeed  $(\boldsymbol{T}^{-1} - \boldsymbol{G}_o)^{-1}$ . Expansion (4) is generally called the MS series expansion.

The study of the convergence of this expansion is therefore important to have a good view of the applicability of this expansion algorithm.

The present work was triggered by the striking results obtained by Osterwalder and his group on Cu(111) and Cu(001) [4]. In this work, simulating photoelectron diffraction using a single scattering (SS) model (order 1 of the MS series expansion) they obtained an excellent agreement with their full-angle experiments for kinetic energies as low as 25 eV whereas it is commonly admitted in the literature that MS series expansion does not converge (or rarely) below 50 eV. We have reproduced their results and found effectively very small differences between the single scattering full angle image and the full MS image based on equation (3). However, simulating the same type of images for TiO<sub>2</sub>(110) at exactly the same kinetic energies led to completely opposite results with no agreement at all between the single scattering approach and the full MS one.

In view of these conflicting results, we decided to investigate in detail the question of the convergence of the MS series so as to have a better comprehension than the one currently provided by the literature.

Our work is organized as follows. In section 2 we give the basic ideas that allow the discussion of the convergence. In particular, we explicit the spectral radius which is the key quantity in our approach. Section 3 is devoted to the analysis of the trends on the variations of the spectral radius as a functions of various structural and electronic structure parameters. As computing a spectral radius takes roughly the same time as performing the full matrix inversion (3), we discuss and test in section 4 various estimates for this quantity. In section 5, we propose a direct application.

## 2. MS series and the spectral radius

From now on, we will refer to MS series expansion as the matrix Taylor expansion

$$(\mathbf{I} - \mathbf{G}_o\mathbf{T})^{-1} = \mathbf{I} + \mathbf{G}_o\mathbf{T} + (\mathbf{G}_o\mathbf{T})^2 + (\mathbf{G}_o\mathbf{T})^3 + \dots \quad (5)$$

where we have dropped the  $\mathbf{T}$  multiplier for simplicity. We will also call the matrix  $\mathbf{G}_o\mathbf{T}$  the kernel matrix, in reference to its role in the Lippmann-Schwinger integral equation.

As  $\mathbf{G}_o\mathbf{T}$  is diagonalizable, we can write it as  $\mathbf{G}_o\mathbf{T} = \mathbf{S}\mathbf{D}\mathbf{S}^{-1}$ , where  $\mathbf{D}$  is a diagonal matrix, so that expansion (5) becomes

$$(\mathbf{I} - \mathbf{G}_o\mathbf{T})^{-1} = \mathbf{S}(\mathbf{I} + \mathbf{D} + \mathbf{D}^2 + \mathbf{D}^3 + \dots)\mathbf{S}^{-1} \quad (6)$$

The expansion in terms of the diagonal matrix  $\mathbf{D}$  converges if, for any eigenvalue  $\lambda_i$  of  $\mathbf{D}$  the expansion

$$(1 - \lambda_i)^{-1} = 1 + \lambda_i + \lambda_i^2 + \lambda_i^3 + \dots \quad (7)$$

is convergent.

Defining the spectral radius  $\rho(\mathbf{G}_o\mathbf{T})$ , i.e. the radius of the spectrum of  $\mathbf{G}_o\mathbf{T}$  as

$$\rho(\mathbf{G}_o\mathbf{T}) = \max_i |\lambda_i| \quad (8)$$

we deduce, as was already recognized by Natoli and Benfatto [5], that the MS series expansion (5) converges provided that the spectral radius  $\rho(\mathbf{G}_o\mathbf{T})$  of the kernel matrix  $\mathbf{G}_o\mathbf{T}$  is smaller than 1. Hence, we can infer that the spectral radius gives some sort of representation of the importance of MS in a system.

We can apply now these results to the two systems we defined in the introduction, Cu(111) and TiO<sub>2</sub>(110). The results are given in figure 1, together with full angle PED calculations both in single scattering (on the left of each subfigure) and using full inversion of equation (3) (on

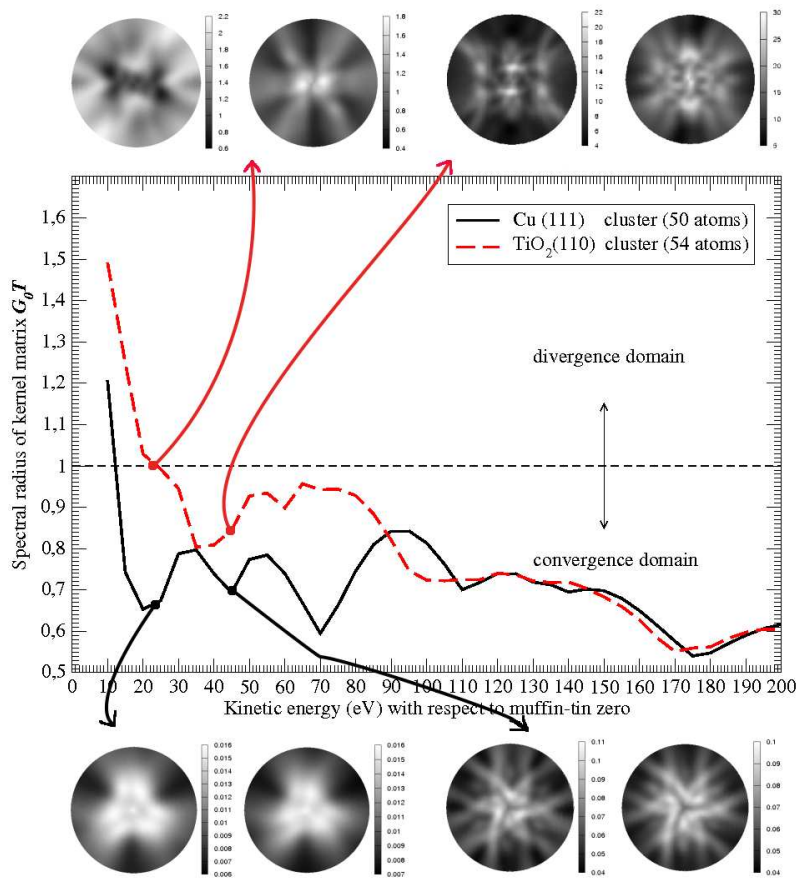


**Figure 1.** Evolution of the spectral radius for Cu(111) and TiO<sub>2</sub>(110). PED calculations corresponding to the Osterwalder’s group experiment [4] are also presented at 25 eV and 45 eV. Lefthand side figures correspond to SS while righthand side ones are computed using full inversion of the MS matrix.

the right of each subfigure). The most striking feature in this result is that the spectral radius does not decrease in a monotonous way as we would have expected, but oscillates. Another interesting feature is that in the first 120 eV, the spectral radii of Cu(111) and TiO<sub>2</sub>(110) are completely different while at higher energies, they are basically identical.

We understand now clearly the intriguing results found by Osterwalder [4] : indeed, both at 25 eV and at 45 eV, the spectral radius is at a minimum and has a low value, therefore inducing a fast convergence of the MS series. In contrast, for TiO<sub>2</sub>(110), the spectral radius is much higher, it is even about 1 at 25 eV, hence the large discrepancy between the SS and full MS.

Let us point out that these calculations and the followings were made with all damping (induced by vibrations and the imaginary part of the Hedin-Lundqvist potential). When damping is removed, the spectral radius is within the divergence domain for both materials.

### 3. Some trends on the variations of the spectral radius

The particular structure of the MS matrix as defined in (3) is extremely interesting as it contains the information on the chemical/electronic structure (the  $T$  matrix) along the diagonal, and the

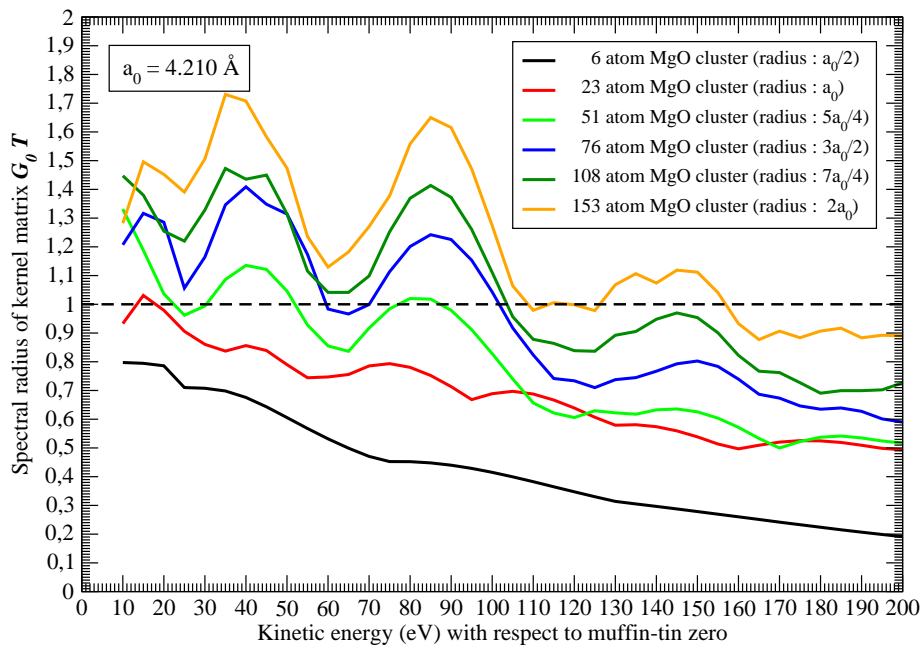


**Figure 2.** Evolution of the spectral radius as a function of the cluster radius.

crystallographic structure (the  $\mathbf{G}_o$  matrix) off diagonal. When inverting it to compute the scattering path operator, or when extracting the eigenvalues of this MS matrix, these two types of information will mix together so that both the spectroscopy considered, and the spectral radius of the kernel matrix will result from an interplay between the crystallographic and the electronic structure. As a consequence, we expect  $\rho(\mathbf{G}_o\mathbf{T})$  to be very sensitive to changes in these structures.

In order to try to disentangle this information and (hopefully) understand the oscillations, we have performed a series of tests on the different parameters that affect the spectral radius.

### 3.1. Cluster size

As the spectral radius  $\rho(\mathbf{G}_o\mathbf{T})$  can be viewed as a measure of the importance of MS in the system under study, we expect its value to increase with the size of the cluster. To assess this trend, we have calculated  $\rho(\mathbf{G}_o\mathbf{T})$  for a MgO(001) cluster whose size is steadily increased. Because of CPU time constraints, we limited ourselves to a cluster radius of twice the lattice parameter.

The results are presented in figure 2. Several remarks can be made about these results. The first one is about the appearance of the oscillations; it is indeed clear from figure 2 that a critical size is necessary for all the oscillations to be present. The second remark, which is what we anticipated, is that indeed  $\rho(\mathbf{G}_o\mathbf{T})$  increases with the cluster size. We see also that this increase can roughly be described as a overall shift, no new structure appearing once the critical size has been reached. This critical size is, in the case of the MgO(001) cluster, of about 50 atoms. The last remark is more a warning. As we explained in the introduction, the kinetic energy of 50 eV is generally taken as a rough boundary between the convergence and the divergence domain of the MS series, and as a consequence, it is commonly admitted that above 75 eV, it is safe to use MS series to model a spectroscopy. Our results on the energy variations of the spectral radius clearly demonstrate that this is wrong as in the case of figure 2, for a 153 atom MgO(001) cluster, there is clearly divergence at 150 eV.

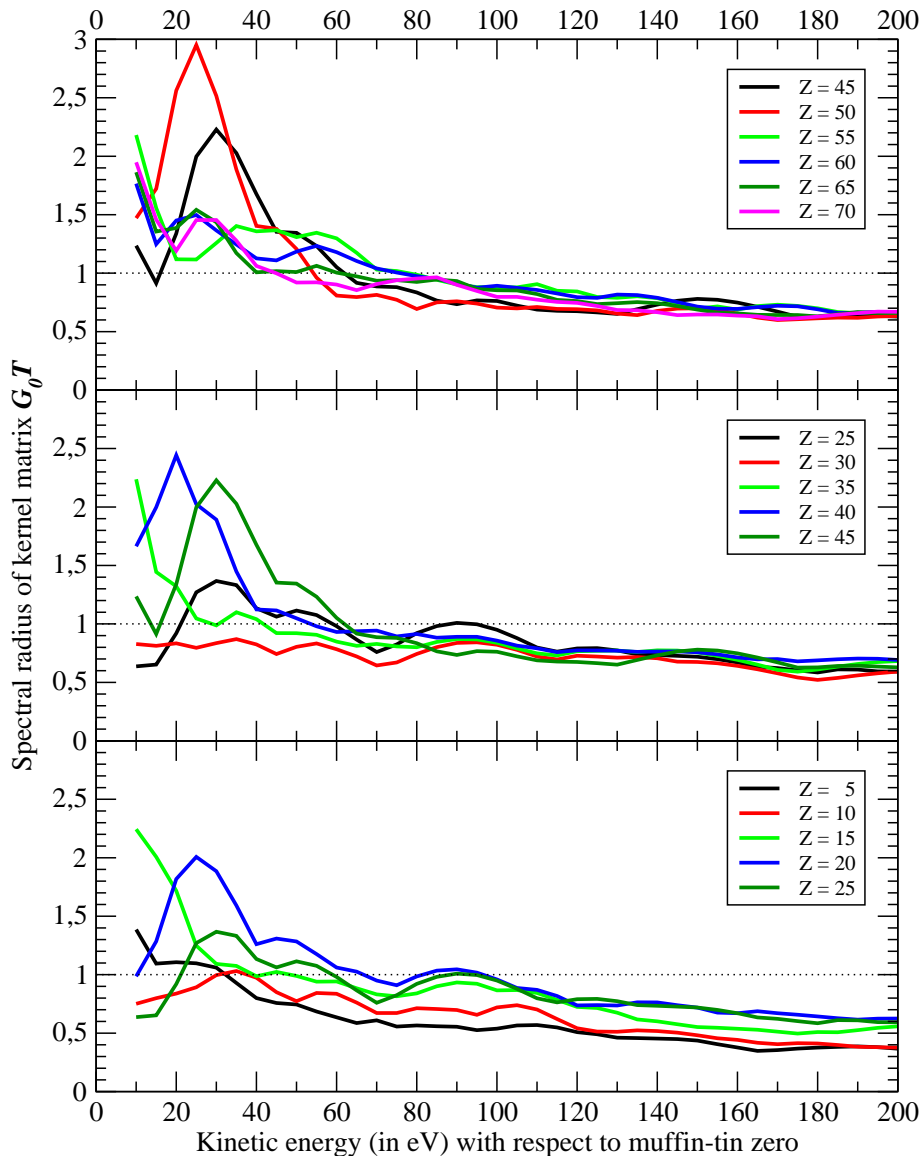


**Figure 3.** Evolution of the spectral radius as a function of the atomic number  $Z$ .

### 3.2. Electronic structure

One of the important parameters that builds up the electronic structure of a material is obviously the chemical species involved. In figure 3, we have computed the spectral radius for atomic numbers  $Z$  ranging from 5 to 70, by step of 5. We used a Cu(111)-like 50 atom cluster and just changed the  $T$  matrix elements using a not self-consistent potential to compute them. Here, we have used the same scale for each plot. What is striking in these results is that the  $t_l$  have a very strong influence on  $\rho(G_o T)$  in the first 50 eV. Then, the influence decreases for larger energies, with the oscillations being slightly modified while their average value, except for very light atoms, is more or less independent of  $Z$ .

Then, we checked the effect of the outer shell part of the potential, choosing for this three elemental solids which are in the same column of the Mendeleev table : Cu, Ag and Au. All crystallize in the FCC crystalline structure so that only the lattice parameter and the potential

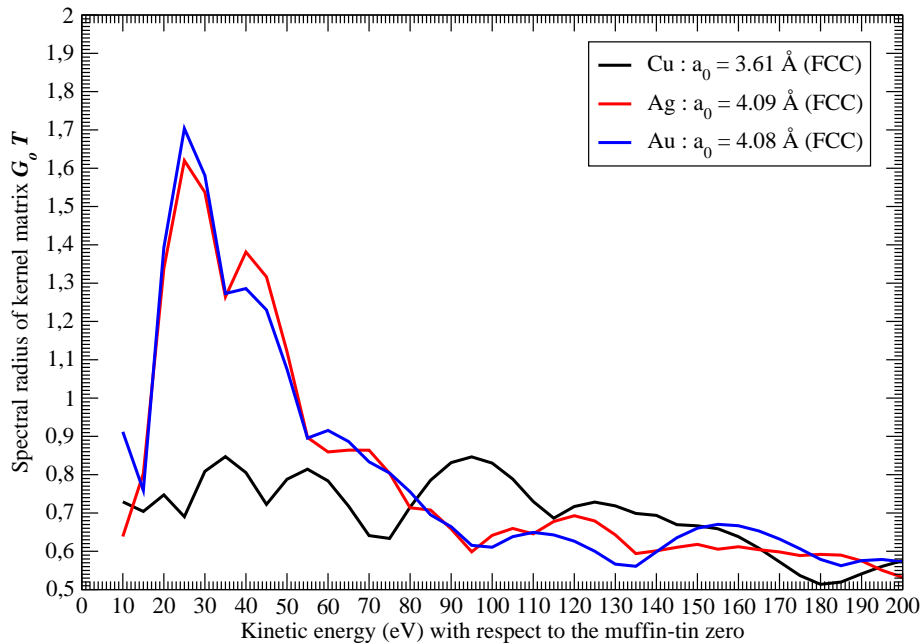


**Figure 4.** Evolution of the spectral radius as a function of the atomic number  $Z$  for the same outer shell structure.

will differ in our comparison. The results are shown in figure 4. They are extremely interesting as we see that for Ag and Au, despite a difference of 32 in the atomic number, the spectral radius is basically the same in the first 100 eV. In this case, both the outer shell configuration and the crystallographic structure are the same (their lattice parameter differs by 0.01 Å). For energies larger than 100 eV on the contrary, the oscillations depend on the  $Z$  number. Therefore, we have here a direct proof of the well-known fact that at low energies, the scattering is essentially due to the outer shell while for large energies it depends almost exclusively on the core structure, i.e. on the atomic number. But, these results also show that, despite being dominated by the outer shell structure at low energies, the crystal structure has also a strong influence in this energy range.

#### 4. Estimates of the spectral radius

Up to now, we have just illustrated some trends followed by the spectral radius. It enables us to deduce some ideas about the variations of  $\rho(\mathbf{G}_o \mathbf{T})$  and its magnitude, and realize that they are quite complex. However, this is not sufficient if we want to better control the convergence of MS series. In this case, we would need to have a knowledge of the spectral radius as exact as possible. Obviously, it is preferable not to compute it exactly, as an eigenvalue calculation on a given matrix takes roughly the same CPU time as the full matrix inversion. We need therefore a reasonable estimate of  $\rho(\mathbf{G}_o \mathbf{T})$ . Furthermore, if we can obtain such an estimate, it could help us shed further light into the oscillations exhibited by the spectral radius as a function of energy. In the following, we review some standard methods to estimate the spectral radius and test them in the Cu(111) case.

##### 4.1. Geršgorin theorem

Geršgorin theorem [6] enjoys a widespread popularity in linear algebra, both because of its beautiful simplicity and its extreme utility.

Let  $\mathbf{A}$  be a matrix whose spectral radius we want to estimate. The Geršgorin discs are defined by

$$\Gamma_i(\mathbf{A}) = \{z \in \mathbb{C}; |z - a_{ii}| \leq R_i^H(\mathbf{A}) = \sum_{j \neq i} |a_{ij}|\} \quad (9)$$

$R_i^H(\mathbf{A})$  is generally called the Geršgorin radius or the Hadamard radius. So, each Geršgorin disc is centered on a diagonal matrix element and has a radius equal to the absolute sum of the off diagonal terms of the corresponding line. Then, Geršgorin theorem simply states that all the eigenvalues of  $\mathbf{A}$  lie within the reunion of the Geršgorin discs. Therefore

$$\rho(\mathbf{A}) \in \bigcup_i \Gamma_i(\mathbf{A}) \quad (10)$$

It is clear that similar discs  $\bar{\Gamma}_i(\mathbf{A})$  can be constructed using the column values instead of the line values of  $\mathbf{A}$ . Therefore, we can restrict the Geršgorin domain which contains all the eigenvalues to the intersection of  $\bigcup_i \Gamma_i(\mathbf{A})$  and  $\bigcup_j \bar{\Gamma}_j(\mathbf{A})$ . It is important to note that the Geršgorin discs are inclusion sets, i.e. sets which contain the eigenvalues.

The Geršgorin discs for our problem being all centered on 0 as  $\mathbf{G}_o\mathbf{T}$  has only zeros on its diagonal, we deduce the Geshgorin estimate for the spectral radius  $\rho(\mathbf{G}_o\mathbf{T})$

$$\rho(\mathbf{G}_o\mathbf{T}) \leq \max_{i, L_i} \left[ \sum_{j \neq i, L_j} |G_{L_j L_i}^{ji} t_{L_i}| \right] \quad (11)$$

#### 4.2. Recent results

The evergrowing interest in computing bounds for the eigenvalues of a matrix has led very recently to some interesting new results.

In the case of non negative matrices, Zhang and Li [7] have proposed two different sorts of lower and upper bounds for  $\rho(\mathbf{A})$ . Noting  $R_j$  the sum of the elements of line  $j$  and introducing the quantities

$$M_i = \sum_j |a_{ij}| R_j, \quad N_i = \sum_j |a_{ij}| M_j \quad \text{and} \quad m_i = \frac{M_i}{R_i} \quad (12)$$

they demonstrate that

$$\left\{ \begin{array}{l} \rho(\mathbf{A}) \leq \max_i \sqrt{M_i} \quad (\text{Zhang-Li 2 approximation}) \\ \rho(\mathbf{A}) \leq \max_i m_i \quad (\text{Zhang-Li 3 approximation}) \end{array} \right. \quad (13)$$

Replacing the max by a min in the previous equations, we obtain the Zhang and Li [7] lower bound.

In figure 5, we have plotted the exact spectral radius versus different approximations. As these approximations are normally defined for positive matrices, we have also plotted  $\rho(|\mathbf{G}_o\mathbf{T}|)$ .

We see clearly from figure 5 that these approximations are disastrous as they lead to variations almost without structures and much higher than the true value. But comparison to  $\rho(|\mathbf{G}_o\mathbf{T}|)$  reveals undoubtedly that they are actually quite good for the type of matrices they were devised for, positive matrices. Actually, we found that by averaging the Zhang-Li upper and lower bound, we could reproduce almost exactly  $\rho(|\mathbf{G}_o\mathbf{T}|)$  in the whole range of energy considered, for a computational cost which is negligible.

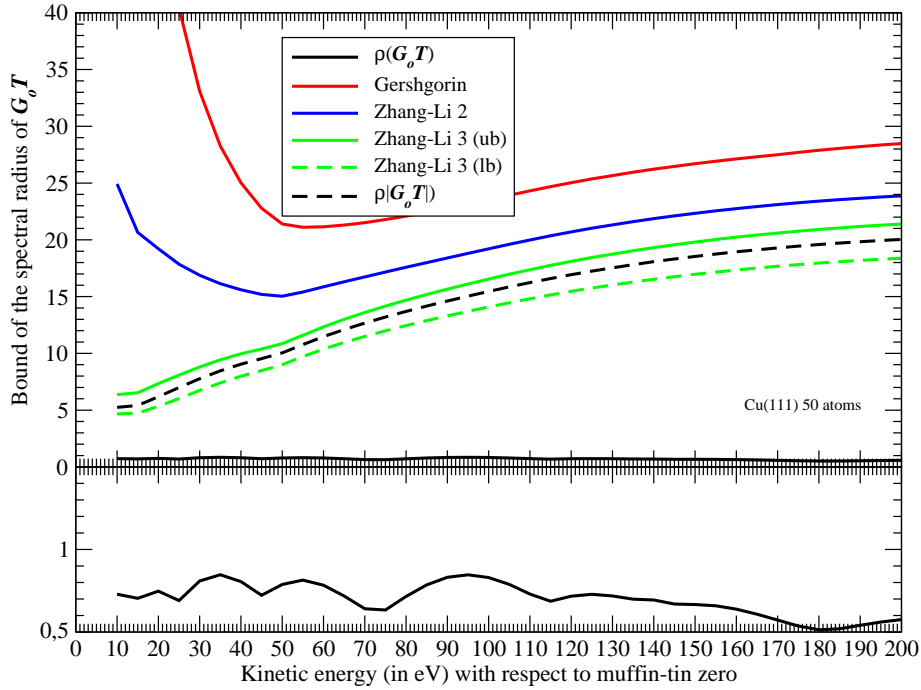


**Figure 5.** Spectral radius  $\rho(\mathbf{G}_o\mathbf{T})$  compared to Gershgorin and Zhang-Li estimates. Here (ub) and (lb) respectively mean upper bound and lower bound. The spectral radius of  $\rho(\mathbf{G}_o\mathbf{T})$  is also given as a comparison.

#### 4.3. Devising better estimates

All the estimates we have tested so far are based on the matrix elements of the modulus matrix  $|\mathbf{A}|$ . We have just seen, by comparing the exact values of  $\rho(\mathbf{G}_o\mathbf{T})$  to those of  $\rho(|\mathbf{G}_o\mathbf{T}|)$ , that the very act of taking the modulus matrix was both pushing up strongly the spectral radius, and suppressing from its energy variations all the structure normally present. It is therefore necessary, in order to obtain better estimates, to use other forms than  $|\mathbf{A}|$  as our starting point.

One possible way to do it, which has been known for a long time, is the power method. It is based on the fact that eventually,  $\frac{\|\mathbf{A}^k \mathbf{x}\|}{\|\mathbf{A}^{k-1} \mathbf{x}\|}$  will tend to the largest eigenvalue, whatever the choice of  $\mathbf{x}$  and the choice of vector norm.

To understand it, let us label the eigenvalues of  $\mathbf{A}$  according to

$$|\lambda_1| > |\lambda_2| \geq |\lambda_3| \geq \dots \geq |\lambda_N| \quad (14)$$

We note  $\mathbf{x}_1, \mathbf{x}_2, \dots, \mathbf{x}_N$  the corresponding eigenvectors. Then, any starting vector can be decomposed over the basis of the eigenvectors

$$\mathbf{x} = \sum_{i=1}^N \alpha_i \mathbf{x}_i \quad (15)$$

It is then straightforward to see, factorizing the largest eigenvalue, that

$$\mathbf{A}^k \mathbf{x} = \lambda_1^k \sum_{i=1}^N \alpha_i \left( \frac{\lambda_i}{\lambda_1} \right)^k \mathbf{x}_i \quad (16)$$

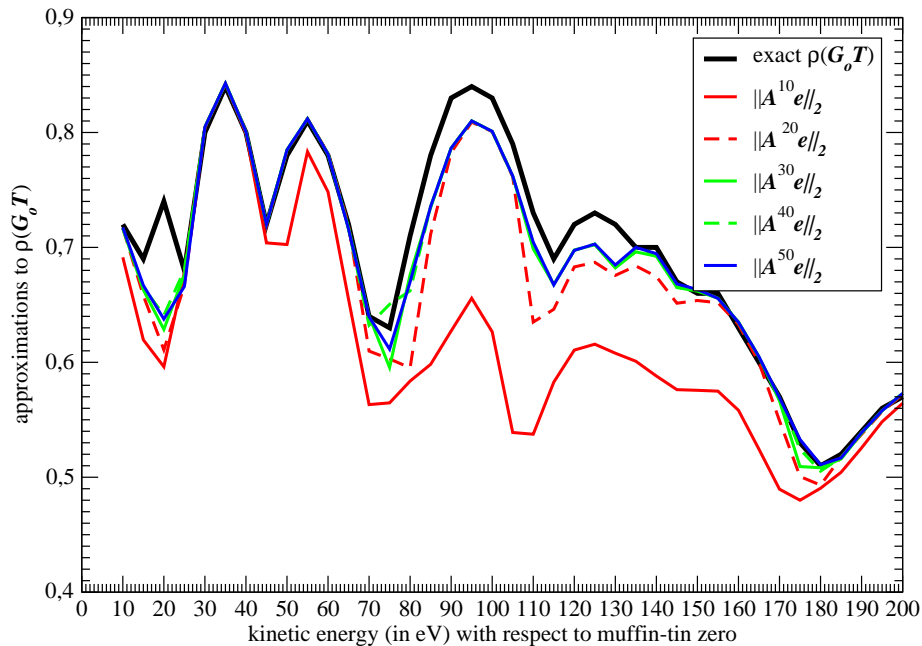


**Figure 6.** Estimates of the spectral radius using the power method for  $\mathbf{e} = (1, 1, \dots, 1)$ .

So, we have

$$\frac{\|\mathbf{A}^k \mathbf{x}\|_2}{\|\mathbf{A}^{k-1} \mathbf{x}\|_2} = |\lambda_1| \sqrt{\frac{\sum_i |\alpha_i|^2 \left| \frac{\lambda_i}{\lambda_1} \right|^{2k}}{\sum_i |\alpha_i|^2 \left| \frac{\lambda_i}{\lambda_1} \right|^{2k-2}}} \quad (17)$$

If  $\lambda_1$  dominates all other eigenvalues, both expressions will tend to  $|\lambda_1|$  when  $k$  tends to infinity. The rate of convergence is given by  $|\lambda_2|/|\lambda_1|$ . So, when this ratio is small, convergence will be faster.

Figure 6 shows the results obtained with this method, using as the starting vector  $\mathbf{e} = (1, 1, \dots, 1)$ . We see that with this method, we can approach quite closely the exact result. There are however a few discrepancies. They occur at energies where  $|\lambda_2|/|\lambda_1|$  is close to 1.

In that case, the trajectory of  $\frac{\|\mathbf{A}^k \mathbf{x}\|_2}{\|\mathbf{A}^{k-1} \mathbf{x}\|_2}$  in the energy plane can jump from the  $|\lambda_1|$  path to the  $|\lambda_2|$  path as can be seen when plotting the energy variations of  $|\lambda_1|$  and  $|\lambda_2|$ . This can be overcome by a better choice of the starting vector  $\mathbf{x}$ . Indeed, if we choose this vector so that  $\alpha_2$  in (15) is very small, then we can prevent the hopping from the  $|\lambda_1|$  path to the  $|\lambda_2|$  path. To check this, we have plotted in figure 7 the results obtained with different simple starting vectors. In addition to  $\mathbf{e}$ , we have used vectors involving a phase change when moving across the coordinates. Here, we have taken  $j$  as the cubic root  $e^{i2\pi/3}$  of unity.

To quantify the gain obtained by using our power method approximation, we have measured the CPU time needed on a desktop computer to perform these iterations as a function of the number of iterations. The CPU times clearly scales linearly with the number of iterations. In our case, with a matrix whose size varies between 800 at 10 eV and 6602 at 200 eV, we take roughly 60 seconds per iteration, plus a time of  $\sim 1500$  s to set up the matrix. By comparison,

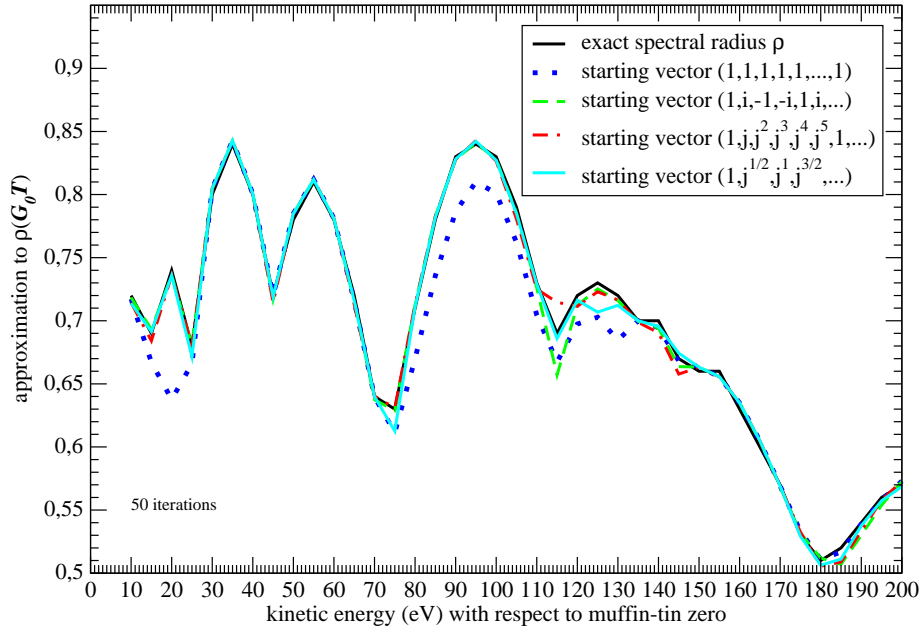


**Figure 7.** Estimates of the spectral radius using the power method for various starting vectors.

the complete calculation of the spectrum, using the corresponding Lapack subroutines, takes about 161000 seconds ! Therefore, even for 40 or 50 iterations, our method is considerably faster than the full calculation.

### 5. Application : estimate of the truncation order

To simplify the notation, let us write  $\mathbf{A} = (\mathbf{I} - \mathbf{G}_o \mathbf{T})^{-1}$ . We can introduce an order  $n$  series expansion approximation of  $\mathbf{A}$  by

$$\mathbf{A}_n = \mathbf{S} (\mathbf{I} + \mathbf{D} + \mathbf{D}^2 + \mathbf{D}^3 + \dots + \mathbf{D}^n) \mathbf{S}^{-1} \quad (18)$$

If we seek an approximation of  $\mathbf{A}$  with an error of  $\epsilon$  at most, we can truncate the series expansion (6) at order  $n$  provided that

$$\|\mathbf{A} - \mathbf{A}_n\| \leq \epsilon \quad (19)$$

where  $\|\cdot\|$  represents any matrix norm.

Using equations (6) and (18), the previous inequality becomes

$$\|\mathbf{S} \mathbf{D}^{n+1} (\mathbf{I} - \mathbf{D})^{-1} \mathbf{S}^{-1}\| \leq \epsilon \quad (20)$$

which can be rewritten as

$$\|(\mathbf{G}_o \mathbf{T})^{n+1} (\mathbf{I} - \mathbf{G}_o \mathbf{T})^{-1}\| \leq \epsilon \quad (21)$$

We can use the norm property

$$\|\mathbf{X} \mathbf{Y}\| \leq \|\mathbf{X}\| \cdot \|\mathbf{Y}\| \quad (22)$$

which is valid whatever the choice of matrix norm. Furthermore, we have [8]

$$\rho(\mathbf{X}^n) = \rho(\mathbf{X})^n \leq \|\mathbf{X}\|^n \quad (23)$$

We can make the choice of the minimum norm for which [9]

$$\rho(\mathbf{X}) = \inf_{\|\cdot\|} \|\mathbf{X}\| \quad (24)$$

so that inequality (19) will always be satisfied if

$$\rho((\mathbf{G}_o\mathbf{T})^{n+1}) (1 - \rho(\mathbf{G}_o\mathbf{T}))^{-1} \leq \epsilon \quad (25)$$

This leads to the condition

$$n \gtrsim \frac{\log [\epsilon(1 - \rho(\mathbf{G}_o\mathbf{T}))]}{\log [\rho(\mathbf{G}_o\mathbf{T})]} - 1 \quad (26)$$

For instance, choosing an accuracy  $\epsilon = 10\%$ , we find for  $\rho(\mathbf{G}_o\mathbf{T}) = 0.9$  that  $n \sim 19$ , while  $n$  drops to  $\sim 3$  if  $\rho(\mathbf{G}_o\mathbf{T}) = 0.5$ .

Because of the approximations we made to devise this estimate, it gives an upper bound of the truncation order. A better estimate, that would allow to quantify the results of figure 1 is under current investigation.

## 6. Conclusion

We have presented a study of the energy variations of the spectral radius of the kernel matrix  $\mathbf{G}_o\mathbf{T}$  in relation to the convergence or divergence of the multiple scattering matrix. We have shown that this spectral radius exhibits strong oscillations which are due both to the crystallographic and the electronic structure through a complex interplay. An important consequence we have to bear in mind is that the spectral radius increases with the size of the cluster. Therefore, in the medium energy range, the use of large clusters might prevent the convergence of the series expansion calculation. The calculation of this radius being almost as long as performing the full MS matrix inversion, we have devised a way based on the power method to approximate it quite accurately. We are currently working on acceleration schemes to further speed up the computation of the spectral radius, and for a better understanding of the oscillations.

## Acknowledgments

We are indebted to Y. Joly and P. Krüger for fruitful suggestions. This work was carried out within the framework of the LighTnet european network.

## References

- [1] Although it was not named, the first mathematical definition of what we call now the scattering path operator seems to have been given by L. D. Faddeev in Faddeev L D 1965, *Mathematical Aspects of the Three-body Problem in the Quantum Scattering Theory* (Israel Program for Scientific Translation: Jerusalem).
- [2] Györffy B L and Stott M J 1973, *Band Structure Spectroscopy of Metals and Alloys* edited by D. J. Fabian and L. M. Watson (Academic Press: London) p 385-403.
- [3] Sébilleau D, Gunnella R, Wu Z-Y, Di Matteo S and Natoli C R 2006, *J. Phys.: Condens. Matter* **18**, R175-R230
- [4] Osterwalder J, Greber T, Aebi P, Fasel R and Schlappbach L 1996, *Phys. Rev. B* **53**, 10209
- [5] Natoli C R and Benfatto M 1986, *J. Phys. (France) C* **8**, 11
- [6] Gerschgorin S 1931, *Izv. Akad. Nauk SSSR Ser. Mat.* **7**, 749  
Salas H N 1999, *Linear Algebra Appl.* **291**, 15
- [7] Zhang X-D and Li J-S 2002, *Acta Mathematica Sinica, English Series* **18**, 293
- [8] Kittaneh F 2005, *Proc. Am. Math. Soc.* **134**, 385
- [9] Czornik A and Jurgaś P 2006, *Int. J. Appl. Math. Comput. Sci.* **16**, 183